



Toward Prebiotic Chemistry on Titan: Impact Experiments on Organic Haze Particles

Ben K. D. Pearce¹ , Sarah M. Hörst¹ , Christopher J. Cline², Mark J. Cintala², Chao He^{1,3} , Joshua A. Sebree⁴ , Shannon M. MacKenzie⁵ , R. Terik Daly⁵ , Alexandra J. Pontefract⁵, and Cara Pesciotta¹

¹ Department of Earth and Planetary Science, Johns Hopkins University, Baltimore, MD 21218, USA; bpearce6@jhu.edu, chaohe23@ustc.edu.cn

² NASA Johnson Space Center, Astromaterials Research and Exploration Science, Mail Code X13, 2101 NASA Parkway, Houston, TX 77058, USA

³ School of Earth and Space Sciences, University of Science and Technology of China, Hefei, People's Republic of China

⁴ Department of Chemistry and Biochemistry, University of Northern Iowa, Cedar Falls, IA, USA

⁵ Applied Physics Laboratory, Johns Hopkins University, Space Exploration Sector, Laurel, MD 20723, USA

Received 2023 November 8; revised 2024 January 26; accepted 2024 February 9; published 2024 March 12

Abstract

Impacts are critical to producing the aqueous environments necessary to stimulate prebiotic chemistry on Titan's surface. Furthermore, organic hazes resting on the surface are a likely feedstock of biomolecules. In this work, we conduct impact experiments on laboratory-produced organic haze particles and haze/sand mixtures and analyze these samples for life's building blocks. Samples of unshocked haze and sand particles are also analyzed to determine the change in biomolecule concentrations and distributions from shocking. Across all samples, we detect seven nucleobases, nine proteinogenic amino acids, and five other biomolecules (e.g., urea) using a blank subtraction procedure to eliminate signals due to contamination. We find that shock pressures of 13 GPa variably degrade nucleobases, amino acids, and a few other organics in haze particles and haze/sand mixtures; however, certain individual biomolecules become enriched or are even produced from these events. Xanthine, threonine, and aspartic acid are enriched or produced in impact experiments containing sand, suggesting these minerals may catalyze the production of these biomolecules. On the other hand, thymine and isoleucine/norleucine are enriched or produced in haze samples containing no sand, suggesting catalytic grains are not necessary for all impact shock syntheses. Uracil, glycine, proline, cysteine, and tyrosine are the most unstable to impact-related processing. These experiments suggest that impacts alter biomolecule distributions on Titan's surface, and that organic hazes co-occurring with fine-grained material on the surface may provide an initial source for further prebiotic chemistry on Titan.

Unified Astronomy Thesaurus concepts: [Astrobiology \(74\)](#); [Pre-biotic astrochemistry \(2079\)](#); [Shocks \(2086\)](#); [Titan \(2186\)](#); [Planetary atmospheres \(1244\)](#); [Planetary science \(1255\)](#); [Complex organic molecules \(2256\)](#)

1. Introduction

The atmosphere of Saturn's moon Titan contains multiple layers of organic haze (Atreya 2007; Hörst 2017). These solid particles are naturally produced in N₂/CH₄-rich atmospheres via chemical reactions initiated by collisions, ultraviolet (UV) radiation, or thermal ionization and dissociation (Trainer et al. 2006; Hörst 2017). Laboratory analogs of these haze particles contain a myriad of biomolecules including the nucleobases of RNA and DNA, as well as amino acids and their intermediates (Sebree et al. 2018; Pearce et al. 2024).

Titan's crust is predominantly water ice, but the surface is also covered in a variety of organic sediments believed to be sourced from the atmospheric hazes (Hörst 2017). Impacts from comets and planetesimals on the icy surface produce melt pools that can survive up to tens of thousands of years (Neish et al. 2018). These postimpact environments are key sites for potential complex prebiotic chemistry. Crater counts on Saturnian moons suggest that hundreds to thousands of impacts producing craters >10 km in diameter have occurred on Titan (Zahnle et al. 2003). However, weathering processes such as eolian infilling and fluvial erosion actively modify Titanian craters, leaving behind only a few dozen craters that have been observed by Cassini RADAR (Hedgepeth et al. 2020). The

Dragonfly mission to Titan will sample impacted materials surrounding Selk crater in the mid-2030s, which will provide some ground truth on the extent of the prebiotic chemistry that occurs on Titan (Barnes et al. 2021). In the meantime, impact simulations on Titan haze particle analogs in the lab can predict what Dragonfly might find.

Most of Titan's observed impact craters are located in the equatorial region where the surface is dominated by organic sands (Hörst 2017). These sand grains are larger than typical haze particles in Titan's atmosphere. For this reason, it is unclear whether these sands are composed of haze material and, if they are, how the material processed into larger particles (Hörst 2017). As the bulk composition of the sand on Titan is unknown, it is unclear what fraction of surface haze particles would be reactive in the impact conditions. For this reason, we mix our experimental organic haze particles with a quartz sand commonly used in impact studies (Cline & Cintala 2022) in order to simulate the physical effects of impact conditions containing both large and small grains.

It is currently unknown how the biomolecule content of organic hazes is modified by the initial shock from impact events. Previous shock experiments investigating impacts on icy planetary or cometary surfaces led to the production of amino acids such as glycine, alanine, α -aminoisobutyric acid, and isovaline (Martins et al. 2013). On the other hand, shock experiments on samples of amino acids and peptides in artificial meteorites and aqueous solutions of amino acids reveal that these molecules can also be destroyed during the

chaos of impact, with survival percentages dependent on shock pressure (Blank et al. 2001; Bertrand et al. 2009). Bertrand et al. (2009) found that amino acids and dipeptides generally had a >30% survival percentage for a shock pressure of 12 GPa, whereas the survival percentage dropped to 0%–4% for 28.9 GPa. Similarly, Blank et al. (2001) found that a significant fraction (~36%–72%) of amino acids in aqueous solution survived shock pressures ranging from 5 to 21 GPa. Finally, experiments simulating the thermal alteration of organics during hypervelocity capture suggest that there may be only slight thermal decomposition of organic samples for these short (e.g., 10 ms) heating events (Bowden et al. 2008).

In this study, we performed impact experiments on simulated Titan organic haze particles and analyzed the shocked material for biomolecule composition using gas chromatography/mass spectrometry/mass spectrometry (GC/MS/MS) methods. Our experimental shock pressures of ~13 GPa are roughly matching or slightly below the average impact velocity (10 km s^{-1}) on Titan’s icy surface (Zahnle et al. 2003) as suggested by shock simulations onto H_2O ice (Kraus et al. 2011). Hydrocode models of planetary surfaces suggest this impact energy will completely melt but not completely vaporize the impact region (Pierazzo et al. 1997).

2. Methods

2.1. Haze Production

Titan haze particle analogs are produced using the Planetary Haze Research (PHAZER) experimental setup (He et al. 2017). This setup contains a vacuum flow system and stainless steel chamber within which an energy source can be applied to simulate UV, cosmic-ray, or lightning chemistry in planetary atmospheres. The energy source we used for this work was a cold plasma discharge, produced by applying a voltage differential of 6000 V between two electrodes. The electrons produced in the plasma collide with the gas mixture, breaking chemical bonds in a similar fashion to shortwave upper atmospheric UV light ($\lesssim 110 \text{ nm}$; Cable et al. 2012; Pearce et al. 2022) and energetic particles (Pearce et al. 2020). This bond-breaking initiates the chemical pathways that lead to the production of organic haze particles. For a schematic of the PHAZER setup, see Pearce et al. (2022).

Our experimental protocol matches that of previous PHAZER studies (He et al. 2018a, 2018b, 2019, 2020a, 2020b; Hörst et al. 2018; Moran et al. 2020; Pearce et al. 2022, 2024). To summarize, we prepared the gas mixtures using high-purity gases (N_2 -99.9997%, CH_4 -99.999%, and CO -99.99%; Airgas). The gases flowed through a cooling coil submerged in liquid nitrogen prior to reaching the reaction chamber to obtain $90 \pm 5 \text{ K}$ atmospheric temperatures (He et al. 2017). We applied a gas flow of 10 standard cubic centimeters per minute and initiated the 170 W m^{-2} cold plasma source, which produces electrons and ions in the 5–15 eV range. The chamber pressure for this experiment was 1.95 Torr.

The organic haze particles were produced using a gas mixture representing Titan’s atmosphere of $\text{N}_2:\text{CH}_4:\text{CO} = 94.8:5:0.2$. Experiments were run for approximately 3 days until an orange-brown powder formed on the walls of the chamber, as seen through the chamber window. We then turned off the plasma source and gas flow, sealed the chamber, and transferred it into a dry ($<0.1 \text{ ppm H}_2\text{O}$), oxygen-free ($<0.1 \text{ ppm O}_2$) N_2 glovebox (I-lab 2GB; Inert Technology),

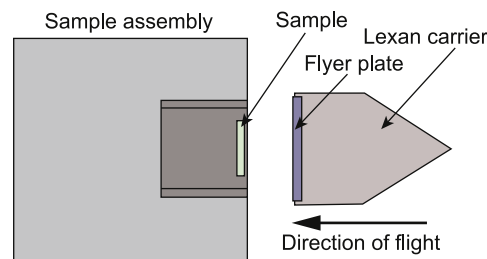


Figure 1. Schematic of sample assembly used in the flat-plate accelerator experiments. Not drawn to scale.

where samples of the orange-brown solid haze particles were collected with sterilized scoopulas from the walls and base of the chamber and stored in small glass vials. Samples were fabricated by mixing the simulated organic haze with powdered novaculite (fine-grained quartzite sourced from Arkansas, USA) in glass vials to yield three different sample compositions of 100%, 50%, and 10% organic haze by mass. Samples were then sealed with parafilm, safely wrapped and secured in an envelope, and express shipped to NASA Johnson Space Center for the shock experiments.

2.2. Shock Experiments

Shock-recovery experiments were performed using the single-stage, gunpowder-driven, flat-plate accelerator that is housed in the Experimental Impact Laboratory at NASA Johnson Space Center. Details regarding the shock-reverberation technique and general hardware used for these experiments can be found in Hörz (1970) and Gibbons et al. (1975). Samples were unpacked, and 100 mg of each mixture was then loosely packed into a tungsten alloy (HD-17, 90% W, 6% Ni, and 4% Cu) inner sample container that was subsequently pressed into a larger stainless steel outer assembly and stored under an atmosphere of 50 mTorr until the time of the experiment (Figure 1).

For each shock experiment, we placed the assembly inside the impact chamber, evacuated the atmosphere to 40 mTorr, and impacted the assembly with an aluminum flyer plate at $\sim 900 \text{ m s}^{-1}$. Peak pressure for each shot was determined using a one-dimensional impedance-matching technique and the Hugoniot for the metals of the flyer plate and sample assemblies. The achieved reverberation pressures for the 100%, 50%, and 10% organic haze samples were 12.9, 12.5, and 13.2 GPa, respectively. The duration of the shocked state for experiments at this scale is from 0.1 to $1 \mu\text{s}$. Photos of the flyer plate immediately before impact were used to determine the tilt angle of the projectile, and all experiments showed maximum tilts of $<2.7^\circ$. After recovering each shocked assembly, the bulk of the metal was machined away to within a few millimeters of the shocked sample (performed slowly so as not to raise the temperature of the sample). The sample assemblies were then wrapped and secured in a box and delivered to Johns Hopkins University. The remaining metal was then manually pried off and the sample removed and stored in glass vials with parafilm. The samples were only exposed to atmosphere briefly (a few minutes) when we opened the assembly and collected the sample. These glass vials were then wrapped and secured in an envelope and brought to the University of Northern Iowa for analysis.

Notably, for all three samples containing haze particles, a viscous substance formed on the outside of the sample

assembly that may have escaped through one or more cracks from the sample interior. An initial GC/MS/MS analysis was performed on the viscous substance—and it was tentatively found to contain biomolecules—however, given its limited quantity, we ran out of the viscous substance before we developed our most accurate blank subtraction GC/MS/MS protocol. Given the large uncertainties in our initial analysis, the biomolecule content of the viscous substance was not included in this work.

2.3. Biomolecule Analysis

Analysis of all samples (haze particles, sand, and mixtures) was performed using GC/MS/MS protocols originally developed in Sebree et al. (2018) and updated in Pearce et al. (2024). GC/MS/MS is a highly selective and sensitive analysis technique that makes use of all three quadrupoles of the Agilent 7000c triple quadrupole GC/MS in order to concentrate and isolate specific molecules of interest. This method differs from extracted ion chromatogram GC/MS analysis, where quantitation ions are extracted from a total ion chromatogram. Instead, the GC/MS/MS technique only searches for one or two species within exclusive ranges of retention times referred to as gates. Within each gate, a selected parent ion is trapped and preconcentrated at the first quadrupole. This is followed by neutral gas collision and fragmentation at the second quadrupole, where finally, the third quadrupole allows only the qualifier and quantifier daughter ions associated with the fragmentation to pass through the detector. This procedure is well suited for analyzing complex mixtures requiring high sensitivity such as those in this study. We note that with this technique the mass spectra for each gate generally only contain one qualifier and one quantifier daughter peak. The only exception to this is when two species are in the same gate due to their similar retention times. In this case, the two quantifiers from the mass spectrum can be used to deduce the relative fraction of the GC peak that belongs to each species (e.g., uracil and proline). Analysis for this work was done in parallel with the early Earth haze analysis performed in Pearce et al. (2024); thus, the standards used to develop calibration curves are the same as in Pearce et al. (2024).

Two standards were analyzed for this work: an industrial-made physiological amino acid standard (Sigma Aldrich) with 27 detectable components at $0.25 \mu\text{mol ml}^{-1}$ biomolecule⁻¹ and a custom-made standard containing seven nucleobases (Sigma Aldrich, all 99.0%). To make the latter standard, we dissolved seven nucleobases in a 0.1 M solution of NaOH at a concentration of 0.5 mg ml^{-1} nucleobase⁻¹. To measure a range of standard concentrations for calibration curves and limits of detection/quantification (LOD/LOQ), we made separate dilutions of these standards of $\frac{5}{100,000}$, $\frac{20}{100,000}$, and $\frac{200}{100,000}$ to use as base concentrations from which we pulled multiple volumes for GC/MS/MS analysis.

The procedure for standard preparation was as follows. First, we pipetted multiple volumes ranging from 5 to 50 μl of each standard dilution into separate GC vials and dried the vials in the oven at 40°C under N₂ flow. After the solutions were dry, we added 100 μl of dichloromethane (CH₂Cl₂) and heated at 40°C under N₂ flow to evaporate any remaining solvent. Next, we added 30 μl of dimethylformamide and 30 μl of N-tert-butyltrimethylsilyl-N-methyltrifluoroacetamide (MTBSTFA) to the vials and allowed the solutions to derivatize for 30 minutes

under N₂ flow at 80°C. Lastly, we diluted samples with 100 μl of CH₂Cl₂ and injected volumes of 0.5, 0.8, 1, and/or 2 μl into the GC triple quad running in MS/MS mode for analysis. Samples took approximately 25 minutes to run. Two procedural blanks were run through the GC/MS/MS prior to each standard run, and the chromatogram of the second blank was subtracted from the standard chromatogram for analysis.

Compound separation was performed using a Restek capillary column (RTX-5MS) with helium flow held at 1.3 ml minute⁻¹. The initial operating temperature was 100°C, with a ramp-up rate of 10°C minute⁻¹ to a final temperature of 270°C that was held for 11.5 minutes. We used collisionally induced dissociation energies in the range of 10–50 eV for GC/MS/MS analysis. The most effective collision energies for the species in each gate were determined in Sebree et al. (2018) by running multiple energies in MS mode and seeing which resulted in the highest daughter mass spectrum peaks. See Table A1 for details on GC gate retention times, ion peaks, and collision energies.

In Figures A1 and A2, we display the calibration curves for nucleobases and amino acids/other biomolecules, respectively. These curves were fit to three to five data points that (a) covered the range of peak areas measured in our samples, (b) provided the lowest χ^2 value for a least-squares linear fit, and (c) had data points above the LOQ. The one exception was urea, for which some samples contained factors of 1.3–5 times greater peak areas than our most concentrated standard. In these cases, we calculated urea concentrations via extrapolation of the calibration curve and suggested the values as upper limits. We placed the peak areas measured in the unshocked haze particle samples on the calibration curves to demonstrate quantification. See the supplement of Pearce et al. (2024) for further details on the standards and Table A2 for further analysis on LOD and LOQ.

Peak areas and uncertainties were calculated using an interactive Python program developed in Pearce et al. (2023). The program automatically detects peaks within user-defined gates and requires the user to select the noise regions in each gate in order to calculate the average noise floor for the area calculation. Uncertainties in the area are automatically calculated by varying the noise floor by ± 1 standard deviation. However, uncertainties in the calculated concentrations within our organic haze particle samples take into account both the uncertainty in the GC peak area and the uncertainty in the calibration curve line of best fit. The visual aspect of the program allows the user to validate whether peaks are at the correct retention times based on the standards. Furthermore, the program determines signal-to-noise ratios (S/Ns), allowing the user to screen out signals below $S/N = 3$. The program is open-source and can be downloaded from Zenodo (Pearce 2023).

Samples were prepared for analysis using the protocols from Pearce et al. (2024). Haze, sand, and sand/haze samples were weighed and dissolved in a 5.0 mg ml⁻¹ 50:50 solution of methanol and acetone. Vials were agitated and then centrifuged at 10,000 rpm for 10 minutes. To encourage further organic dissolution and separation, vials were rotated 180° and centrifuged again for an additional 10 minutes. Then, we used a Pasteur pipette to transfer the supernatants to GC vials. Next, we dried and derivatized the solutions using the same methods described for the standards above. We injected 1 μl of the solutions into the GC triple quad running in MS/MS mode for

analysis. Two blank solutions of 50:50 methanol/acetone were carried through the same procedure and ran through the GC/MS prior to each sample run. We subtracted the blank chromatogram that was run directly prior to each sample chromatogram for analysis. This procedure was developed in this way due to a comprehensive noise analysis performed in Pearce et al. (2024), which revealed that underivatized biomolecules from the standards can get trapped in the GC inlet and become derivatized and released into the GC column upon subsequent blank or sample runs. Trapping cannot be completely diminished due to the <100% derivatization efficiency of biomolecule samples, as well as the derivatization decay that occurs while the samples are transported to the GC/MS or waiting in the rotating sample queue for GC/MS/MS analysis.

In Pearce et al. (2024), we performed two contaminant analyses to test whether this trapping occurs. First, after a standard was run through the GC/MS, we ran 17 consecutive blanks containing derivatizing agents. From this test, we found that the standard peaks decreased with each additional run, indicating that this procedure slowly washes/removes underivatized biomolecules out of/from the inlet. In no case did a subsequent wash run produce higher peaks than the previous run. Second, we ran blanks without derivatizer and found no contaminant peaks, suggesting that underivatized biomolecules are derivatized and able to vaporize out of the inlet when derivatizer is present in the blank run. Because we cannot completely remove the contaminant peaks from procedural blank runs containing derivatizer, two blanks are run before each sample to wash the inlet, and then the second blank chromatogram is subtracted from the sample chromatogram prior to analysis.

3. Results

In Figure 2, we display the GC/MS/MS chromatograms for the six samples in this study. We shocked three haze samples, containing (A) 100% haze particles, (B) 50:50 haze:sand, and (C) 10:90 haze:sand. We also analyzed unshocked haze particles, as well as unshocked and shocked sand samples. We detected seven nucleobases, nine proteinogenic amino acids, and five other organics (e.g., urea) across all samples. We summarize the detected biomolecules and their concentrations in Table 1.

Unexpectedly, we detected a sulfur-containing amino acid, cysteine, in the unshocked haze sample right at the LOD ($S/N = 3.3$). We did not purposefully introduce sulfur into the gas mixture for the Titan haze production experiments. It is possible that this small peak is a non-sulfur-containing molecule with similar parent and daughter ions as cysteine. However, it is also possible that cysteine was produced in our atmospheric haze experiments from small sulfur impurities in our gas mixtures. It is unlikely that this peak is contaminant introduced during sample preparation or by the GC inlet, as both blank chromatograms run prior to this sample showed no peak at the cysteine retention time.

In Figure 3, we display the nucleobase mass abundances with respect to the sample mass (i.e., haze particles, sand particles, or haze/sand mixture). The unshocked haze particles have the highest summed nucleobase abundances. Individual mass fractions range from 2 to 127 ppm by mass. Shocking haze particles reduces the total nucleobase concentrations within them by a factor of ~ 3 –6. However, we see slight

increases of individual nucleobase concentrations such as thymine and xanthine from shocking two samples: thymine by a factor of 1.4 in the 100% shocked haze sample and xanthine by a factor of 1.7 in the 10:90 shocked haze:sand sample (compared to the unshocked haze). Uracil is the most unstable nucleobase to impacts, as it was undetected in any shocked sample.

Unshocked quartz sand contains thymine, xanthine, and hypoxanthine concentrations at factors of 1.2–2.1 lower than the unshocked haze sample. However, we only detected xanthine and hypoxanthine in the shocked sand sample, and they were depleted in concentration by a factor of 1.1–1.5 with respect to the unshocked sand sample. For future shock experiments of haze particles, it will be beneficial to sterilize the sand prior to mixing it with the haze samples.

Lastly, although we do not include a biomolecule analysis of the viscous substance that formed on the outside of the shock assembly for the samples containing organic haze particles, we weighed the viscous substance and found it to be $\sim 2\%$ of the mass of the shocked haze. We suggest that the viscous substance is likely an escaped by-product of haze material interacting with substances found inside the impact chamber during a shot, such as combusted gunpowder and molten lexan.

In Figure 4, we display the proteinogenic amino acid abundances in the unshocked and shocked samples in this study. Abundances range from 0.35 to 91 ppm by mass. Shocking haze samples also reduces total amino acid content by a factor of 3–8. Glycine, proline, cysteine, and tyrosine are the most unstable to shocks, as we did not detect them in any of the shocked haze samples. On the other hand, we detected isoleucine/norleucine, aspartic acid, and threonine in the 100% haze or 50:50 shocked haze:sand samples but not in the unshocked haze sample. This suggests that these three amino acids are products of shocking organic haze particles.

In Figure 5, we display the abundances of non-proteinogenic amino acids, as well as amino acid derivatives and metabolites in the six samples in this study. The unshocked haze sample has the highest abundances of these organics, ranging from 0.44 to <4692 ppm by mass. Similar to nucleobases and amino acids, shocking the haze samples reduces the total content of these biomolecules by a factor of ~ 5 –6. Sarcosine, β -alanine, and hydroxyproline are the least stable to impacts, as we did not detect them in any of the shocked samples.

4. Discussion

Our experiments suggest that the biomolecules anticipated to be in Titan's organic hazes are generally reduced in concentration when subjected to shock pressures of ~ 13 GPa. On the other hand, some individual nucleobases and amino acids are enriched or produced from the high-temperature and high-pressure conditions of our impact experiments.

Martins et al. (2013) performed shock experiments on ice mixtures analogous to those found in a comet (e.g., $\text{NH}_4\text{OH}:\text{CO}_2:\text{CH}_4\text{OH}$) and found that several amino acids were produced, including glycine, alanine, and norvaline. These results contrast ours, as we only detected norvaline out of these three species in any of our shocked organic haze experiments and in lower concentrations than measured in the unshocked haze particles.

Impact experiments on amino acids in saponite clay showed that norvaline, glycine, aspartic acid, and serine were fairly stable to 12–15 GPa shocks (Bertrand et al. 2009). Similarly,

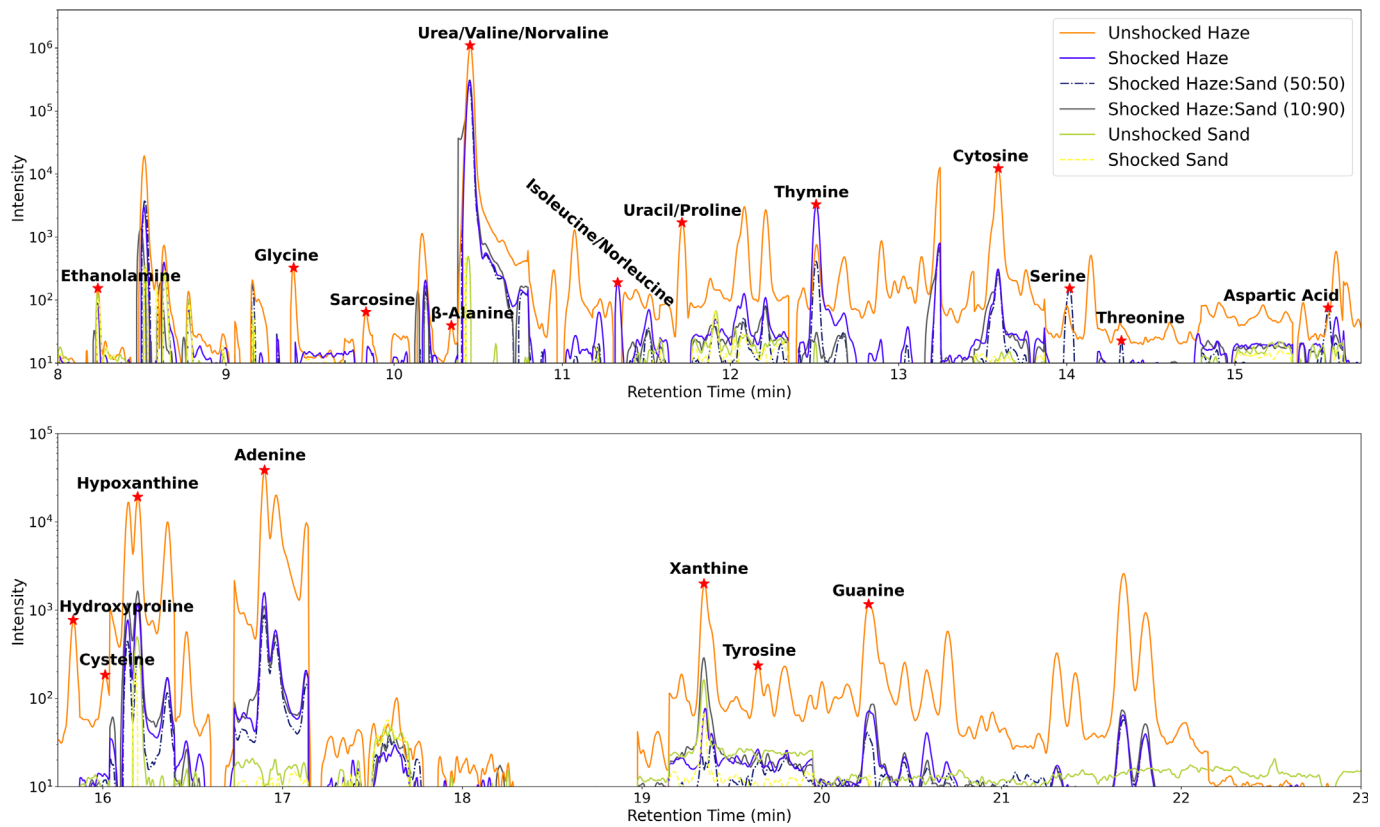


Figure 2. Blank-subtracted GC/MS/MS chromatograms for the six shocked and unshocked samples in this study.

Table 1
Measured Mass Fractions of Nucleobases, Amino Acids, and Other Organics in Shock Experiments

Biomolecule	Unshock. Haze	Shock. Haze	Shock. H:S 50:50	Shock. H:S 10:90	Unshock. Sand	Shock. Sand
Nucleobases						
Adenine	127_{-2}^{+17}	$7.5_{-0.1}^{+2.0}$	$6.7_{-0.2}^{+2.7}$	$5.6_{-0.3}^{+2.5}$
Cytosine	58_{-4}^{+2}	$2.7_{-0.1}^{+0.4}$	$3.7_{-0.1}^{+0.1}$	$2.6_{-0.1}^{+0.3}$
Guanine	$44.8_{-2.3}^{+0.4}$	19_{-1}^{+4}	17_{-2}^{+3}	20_{-1}^{+4}
Hypoxanthine	$38.6_{-0.1}^{+0.6}$	$27.1_{-0.1}^{+1.5}$	$19.8_{-0.2}^{+0.2}$	$33.8_{-0.1}^{+1.3}$	$18.3_{-0.1}^{+1.1}$	$16.3_{-1.3}^{+0.2}$
Xanthine	$30.8_{-0.4}^{+4.7}$	$11.3_{-0.6}^{+3.8}$...	51_{-1}^{+3}	$26.1_{-0.1}^{+3.5}$	17_{-1}^{+6}
Uracil	$5.0_{-1.2}^{+0.1}$
Thymine	$2.1_{-0.5}^{+0.0}$	$2.9_{-0.3}^{+0.0}$	$1.84_{-0.32}^{+0.01}$...	$1.155_{-0.001}^{+0.001}$...
Protein. Amino Acids						
Tyrosine	91_{-15}^{+31}
Valine/norvaline	80_{-0}^{+0}	$24.5_{-0.6}^{+0.0}$	47_{-2}^{+0}	$25.9_{-0.8}^{+0.0}$
Cysteine	$<11.1_{-0.5}^{+0.5}$
Proline	$1.80_{-0.26}^{+0.03}$
Glycine	$0.78_{-0.01}^{+0.21}$
Isoleucine/norleucine	...	$<0.35_{-0.07}^{+0.08}$
Aspartic acid	8_{-1}^{+1}
Threonine	$7.6_{-0.4}^{+0.0}$
Serine	$6.5_{-0.1}^{+0.1}$...	$7.4_{-1.0}^{+0.1}$
Other Biomolecules						
Urea	4692_{-2}^{+2}	791_{-0}^{+0}	948_{-0}^{+0}	977_{-1}^{+1}	$6.24_{-0.01}^{+0.01}$...
Sarcosine	$<12.1_{-0.3}^{+0.3}$
Hydroxyproline	$9.4_{-1.2}^{+2.3}$
β -alanine	$<0.53_{-0.07}^{+0.07}$
Ethanalamine	$0.44_{-0.02}^{+0.03}$	$0.18_{-0.01}^{+0.01}$	$0.37_{-0.01}^{+0.01}$	$<0.06_{-0.01}^{+0.01}$	$0.27_{-0.01}^{+0.02}$	$<0.30_{-0.02}^{+0.02}$

Notes. Uncertainties are the combination of GC peak area uncertainties and the calibration curve uncertainties. A few values are upper bounds, as their GC peak measurements fall between the LOD and LOQ. See Table A2 for more detail. Units are μg biomolecule g^{-1} sample, or ppm.

^a Upper limit based on upper bound extrapolation of calibration curve.

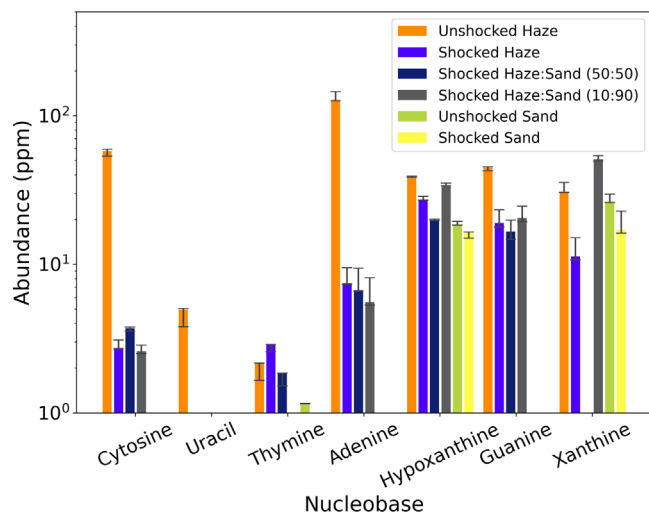


Figure 3. Nucleobase abundances measured in the six shocked and unshocked samples in this study. Nucleobase order is from lowest to highest molar mass. Uncertainties are the combination of GC peak area uncertainties and the calibration curve uncertainties. Comparisons can be made between any two samples, as units are μg biomolecule g^{-1} sample (e.g., haze, sand, or haze/sand), or ppm.

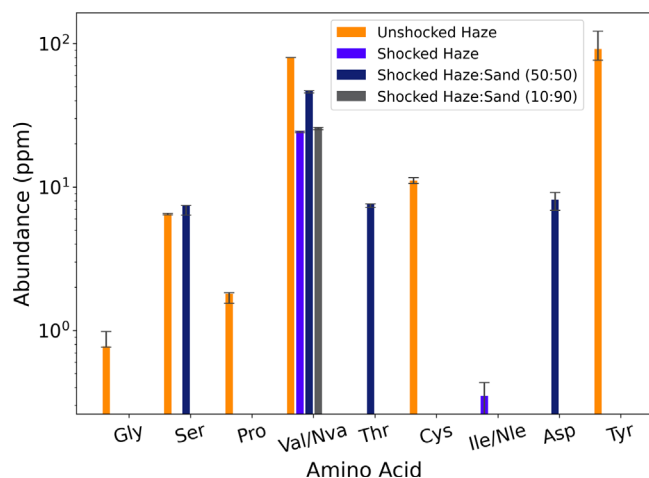


Figure 4. Proteinogenic amino acid abundances measured in the shocked and unshocked samples in this study. Amino acid order is from lowest to highest molar mass. Uncertainties are the combination of GC peak area uncertainties and the calibration curve uncertainties. Comparisons can be made between any two samples, as units are μg biomolecule g^{-1} sample (i.e., haze, sand, or haze/sand), or ppm.

impact experiments on amino acids in solution showed norvaline to be one of the most stable species and proline to be fairly stable (Blank et al. 2001). This is fairly consistent with our results, as we detected norvaline in all of our shocked haze samples, as well as aspartic acid and serine in at least one of our shocked haze samples. However, we did not detect glycine or proline in any of our shocked haze samples. Overall, we do expect there to be discrepancies between impact experiments performed at different pressures and scales. For example, impact experiments by Bowden et al. (2009) found that concentrations in impact ejecta vary with respect to sample location.

In recent biomolecule analyses of organic hazes heated to 200°C , uracil was the only nucleobase that survived (albeit reduced by a factor of 2) of the seven studied nucleobases after

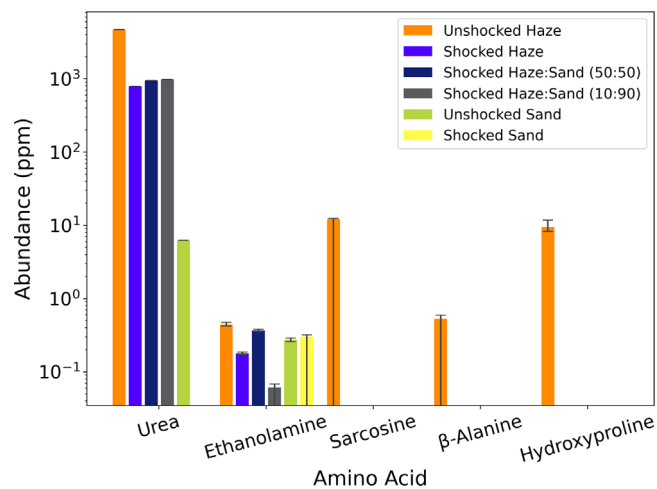


Figure 5. Other biomolecule abundances measured in the shocked and unshocked samples in this study. Amino acid order is from lowest to highest molar mass. Uncertainties are the combination of GC peak area uncertainties and the calibration curve uncertainties. Comparisons can be made between any two samples, as units are μg biomolecule g^{-1} sample (i.e., haze, sand, or haze/sand), or ppm.

7 days (Pearce et al. 2024). This contrasts our results, which show that uracil is the most unstable nucleobase in regard to withstanding shocks. This discrepancy suggests that thermal degradation at 200°C and shock degradation affect nucleobases differently. We did not use a thermocouple to measure the peak temperatures from our shock experiments, and given that the shock wave bounces between the metal that sandwiches the sample, it is too difficult to provide an accurate temperature estimate; however, if it is greater than 200°C , this could be the reason for the differences in the degradation of nucleobases between these two experiments.

There were no increases to nucleobase or amino acid concentrations in the haze particle heating experiments in Pearce et al. (2024). However, in this study, thymine and isoleucine/norleucine were enriched/produced in the 100% haze shock experiment, and xanthine, threonine, and aspartic acid were enriched/produced in haze:sand shock experiments. This suggests that the high-pressure, high-temperature environment created by impacts, as well as the potentially catalytic behavior of quartz sand, provides distinct conditions for the production and modification of biomolecules in organic hazes.

Quartz sand may have catalytic effects on the chemistry of biomolecules in organic hazes when subjected to impacts. This is most obvious in the 50:50 haze:sand shock experiments, which produced threonine and aspartic acid. This could be due to mineral adsorption, which is known to catalyze a variety of organic reactions (Hashizume 2015) and stabilize amino acids and nucleobases against degradation (Poggiali et al. 2020). Experiments by Hashizume et al. (2010) showed that absorption of nucleobases by montmorillonite decreases in the order adenine > cytosine > uracil. Thus, we might expect better survivability of adenine and cytosine over uracil in our haze/sand mixture experiments, which is indeed the case. It is unclear whether the large sand particles that are typical for the equatorial regions on Titan would produce similar catalytic effects as we see here, given that their composition is presently unknown.

It is likely that shocking our haze particle samples is simply breaking biomolecule bonds. However, one alternative possibility worth noting is that shocking these molecules can also

lead to the formation of complex macroscale structures. Shock tube experiments by Singh et al. (2020) found that amino acids tend to form complex agglomerate structures when subjected to 1–3 MPa shocks and 2500–8000 K for 1–2 ms.

Finally, we note two caveats to our experiments. (1) Our experiments were performed without any water in the sample assembly. This is not completely analogous to Titan’s icy surface, and we might expect the inclusion of water to modify the biomolecule distributions further (e.g., oxidation). (2) Reaction catalysis on the surface of the sample assembly cannot be completely discounted. However, we note that the surface area of the sample assembly is small in comparison to the volume of the sample or the surface area of the sand grains.

5. Conclusions

In this work, we performed impact experiments on simulated Titan organic haze particles and haze/sand mixtures and measured the biomolecule content using GC/MS/MS.

The four major conclusions are as follows:

1. The nucleobases, amino acids, and other biomolecules detected in our simulated Titan haze particles degrade overall when shocked at 13 GPa by factors of 3–8. However, in some cases, certain individual biomolecules, i.e., thymine, xanthine, isoleucine/norleucine, threonine, and aspartic acid, are enriched by or even produced from these shocks. This suggests shock synthesis pathways for these species.
2. Uracil, glycine, proline, and tyrosine in haze particles did not survive any impact experiment, suggesting they are the most unstable to these events. This could be because these species react more rapidly than the other species at the temperatures and pressures of our tested shock conditions.
3. Quartz sand may offer catalytic effects for the shock production of threonine and aspartic acid and the enrichment of xanthine in organic haze particles.

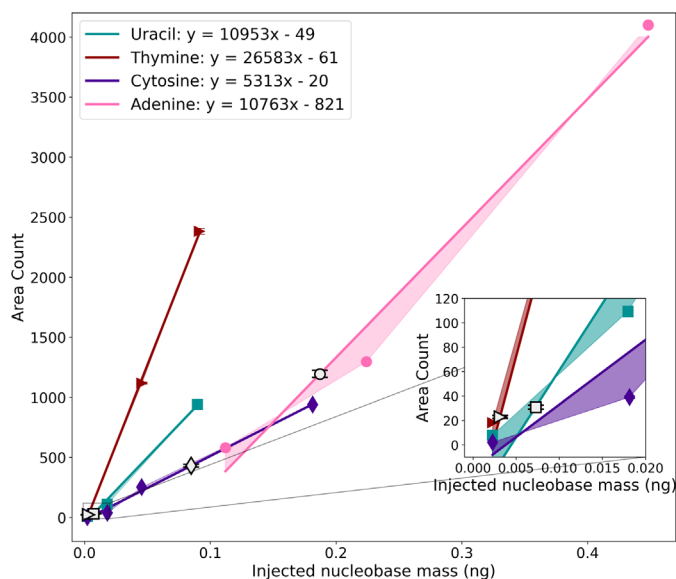


Figure A1. Calibration curves for seven nucleobases. The equations of the lines of best fit are included in the plot legends. Uncertainties are displayed as shaded regions and are calculated using the variance from a model linearly connecting each data point. As an example calculation, we add the peak areas from the GC/MS/MS analysis of the unshocked haze particles.

4. Thermal and shock processes affect nucleobase degradation differently. This may be due to the different thermal histories of shock processes and standard heating processes.

These experiments are the first attempts to understand the effects of impacts on simulated Titan organic hazes. We intend to expand upon these experiments to further understand and characterize the changes in biomolecule distributions from impacts on Titan’s surface. This may involve expanding upon the studied biomolecules, improving upon sterilization procedures, and including water ice in impact experiments.

Acknowledgments

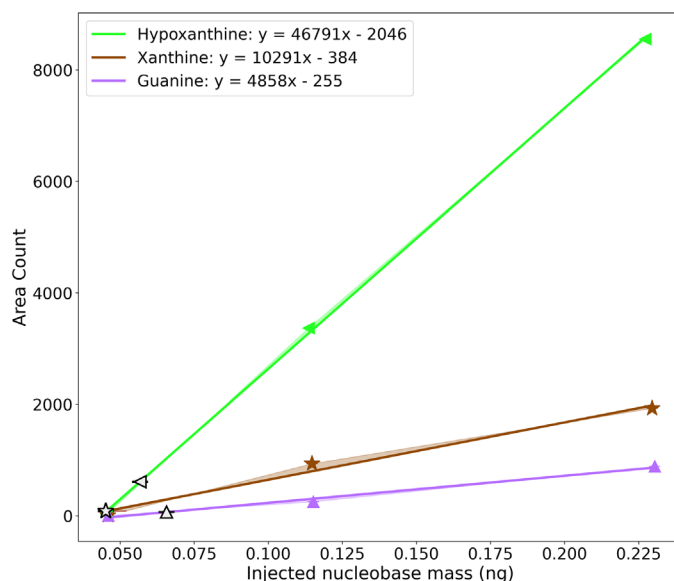
We thank the two anonymous referees, whose comments led to improvements in this paper. B.K.D.P. is supported by the NSERC Banting Postdoctoral Fellowship.

Appendix Supporting Information

In Table A1, we list the details of the GC/MS/MS gates for the detection of nucleobases, amino acids, and other biomolecules in this study. For each range of retention times (gate), only the parent ion is trapped at the first quadrupole, and, after collision and ion fragmentation at the second quadrupole, only the qualifier and quantifier daughter ions are let through the detector. The retention times and collision energies for these species were developed in Sebree et al. (2018); not all of these species are detected in the haze particle samples in this study.

In Figures A1 and A2, we display the calibration curves for the quantification of nucleobases and amino acids/other biomolecules, respectively.

In Table A2, we list the biomolecule injection masses calculated for all of our samples based on their GC peak areas and compare them to the LOD and LOQ roughly constrained by our calibration curve data. The LOD is defined as the lowest



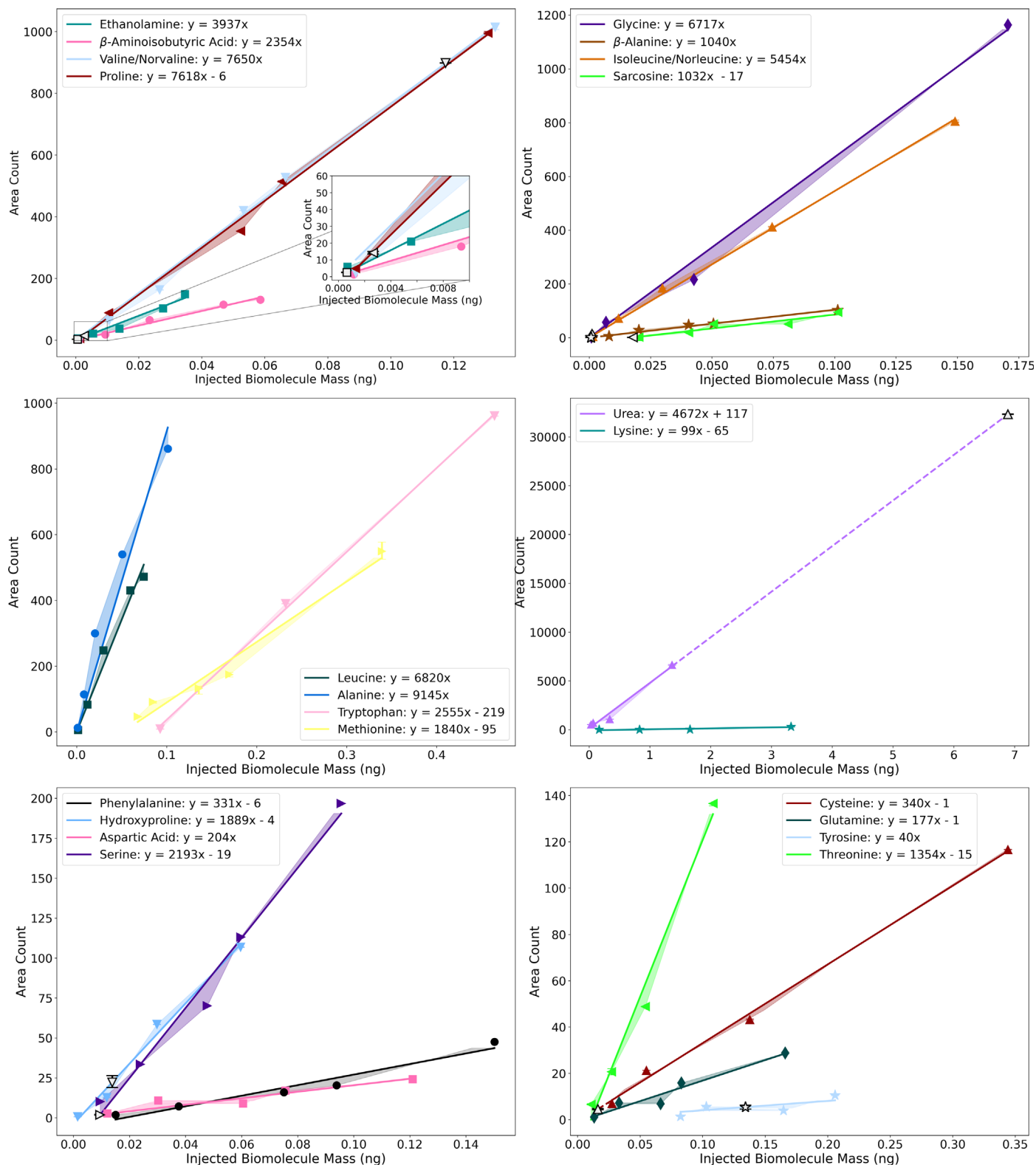


Figure A2. Calibration curves for 22 amino acids and other biomolecules. The equations of the lines of best fit are included in the plot legends. Uncertainties are displayed as shaded regions and are calculated using the variance from a model linearly connecting each data point. As an example calculation, we add the peak areas from the GC/MS/MS analysis of the unshocked haze particles.

injection mass capable of producing a signal with $S/N \sim 3$, and the LOQ is defined as the lowest injection mass capable of producing a signal with $S/N \sim 10$. Given that most of the calibration curve data have $S/N > 10$, we can often only provide upper bounds on the LOQ. When a biomolecule peak

falls below the rough upper bound LOQ or LOD, we also display the S/N for that peak.

All of the sample nucleobase detections are above the upper bound LOQs. However, two proteinogenic amino acid detections and a few other biomolecule detections are below

Table A1
Gate Retention Times, Parent Ions, and Qualifier and Quantified Daughter Ions and Their Respective Collision Energies for GC/MS/MS Detection of the Biomolecules in This Study

Gate	Retention Time Range (minutes)	Biomolecule	Parent Ion (m/z)	Daughter Ions (m/z)	Collision Ener. (eV)
1	8.15–9.05	Ethanolamine	232	147, 116	10, 10
2	9.05–9.3	Alanine	158	102, 73	10, 10
3	9.3–9.7	Glycine	218	189, 147	10, 10
4	9.7–9.87	Sarcosine	260	232, 147	10, 10
5	9.87–10.23	β -aminoisobutyric acid	246	147, 133	10, 10
6	10.23–10.38	β -alanine	260	218, 147	5, 20
7	10.38–10.8	Urea	231	173, 147	15, 15
	10.38–10.8	Valine/norvaline	186	130, 73	12, 15
8	10.8–11.18	Leucine	200	157, 73	15, 20
9	11.18–11.58	Isoleucine/norleucine	200	157, 144, 73	15, 10, 20
10	11.58–12.35	Proline	184	128, 73	15, 25
	11.58–12.35	Uracil	283	169, 99	30, 20
11	12.35–13.25	Thymine	297	113, 73	25, 25
12	13.45–13.87	Cytosine	282	212, 98	20, 25
	13.45–13.87	Methionine	218	170, 73	10, 15
13	13.87–14.18	Serine	288	100, 73	20, 20
14	14.18–14.8	Threonine	303	202, 73	20, 20
15	14.8–15.35	Phenylalanine	336	308, 73	10, 20
16	15.35–15.65	Aspartic Acid	418	390, 73	10, 20
17	15.65–15.87	Hydroxyproline	314	182, 73	10, 20
18	15.87–16.04	Cysteine	304	118, 73	20, 20
19	16.04–16.4	Hypoxanthine	307	193, 73	20, 25
20	16.4–16.73	Glutamine	432	272, 147	15, 15
21	16.73–17.15	Adenine	306	192, 73	10, 25
22	17.15–18.97	Lysine	431	300, 73	10, 15
23	19.15–19.95	Tyrosine	466	438, 147	10, 15
	19.15–19.95	Xanthine	437	363, 73	20, 25
24	19.95–22.15	Guanine	436	322, 73	25, 30
25	22.15–24.35	Tryptophan	244	188, 73	10, 20

Note. Gates were developed in Sebree et al. (2018), and thus not all of these species are detected in the haze particle samples in this work.

the upper bound LOQs. The aspartic acid detection has an S/N of 21, suggesting this detection is above the true LOQ. The isoleucine/norleucine and cysteine detections have S/N s of 8 and 3.3, respectively; therefore, we display these detections

as upper limits in Table 1. Similarly, the β -alanine and sarcosine detections and two of the ethanolamine detections have $3 < S/N < 10$; thus, we also treat these detections as upper limits.

Table A2
Injection Masses Measured for Each Sample in Comparison to LOD, i.e., S/N ~ 3, and LOQ, i.e., S/N ~ 10

Biomolecule	Unshock. Haze	Shock. Haze	Shock. H: S 50:50	Shock. H: S 10:90	Unshock. Sand	Shock. Sand	LOD	LOQ
Nucleobases								
Adenine	187	16	10	12	<2	<2
Cytosine	85	6	6	6	<2	<2
Guanine	66	41	25	45	<2	~18
Hypoxanthine	57	58	30	75	37	23	<18	~18
Xanthine	45	24	...	113	52	25	<2	<2
Uracil	7	<2	<2
Thymine	3	6	3	...	2.3	...	<2	<2
Proteinogenic Amino Acids								
Tyrosine	134	<82	<82
Valine/norvaline	117	53	70	58	<1.3	<11
Cysteine	16 (S/N = 3.3)	<28	<28
Proline	3	<1.3	<1.3
Glycine	1.1	<0.85	<0.85
Isoleucine/norleucine	...	0.8 (S/N = 8)	<1.5	<1.5
Aspartic acid	12 (S/N = 21)	~12	<30
Threonine	11	<11	~11
Serine	10	...	11	<10	<10
Alanine	<1	<1
Leucine	<1.5	<1.5
Hydroxyproline	<1.5	<12
Phenylalanine	<15	<15
Glutamine	<13	<13
Methionine	<68	<68
Cysteine	<28	<28
Tyrosine	<82	<82
Lysine	<166	<166
Other Biomolecules								
Urea	6891	1706	1422	2167	12.5 (S/N = 41)	...	<14	<34
β -alanine	0.8 (S/N = 3.2)	<8	<8
Sarcosine	18 (S/N = 4)	<20	<20
Ethanolamine	0.65 (S/N = 11)	0.4 (S/N = 11)	0.55 (S/N = 42)	0.13 (S/N = 8)	0.55 (S/N = 11)	0.43 (S/N = 9.4)	<0.7	<0.7
β -aminoisobutyric acid	<1.2	<9

Note. The LOD and LOQ are roughly constrained by the lower calibration curve data. Often, only upper bound LOD or LOQ are possible, as the S/N for the lowest standard concentration was often >3 or >10, respectively. In the cases where the injection masses for our samples are lower than the upper bound LOD or LOQ, we display the S/N for that measurement.

ORCID iDs

Ben K. D. Pearce  <https://orcid.org/0000-0002-5449-4195>
 Sarah M. Hörst  <https://orcid.org/0000-0003-4596-0702>
 Chao He  <https://orcid.org/0000-0002-6694-0965>
 Joshua A. Sebree  <https://orcid.org/0000-0001-9612-8532>
 Shannon M. MacKenzie  <https://orcid.org/0000-0002-1658-9687>
 R. Terik Daly  <https://orcid.org/0000-0002-1320-2985>
 Cara Pesciotta  <https://orcid.org/0009-0007-6910-6347>

References

Atreya, S. 2007, *Sci*, 316, 843
 Barnes, J. W., Turtle, E. P., Trainer, M. G., et al. 2021, *PSJ*, 2, 130
 Bertrand, M., van der Gaast, S., Vilas, F., et al. 2009, *AsBio*, 9, 943
 Blank, J. G., Miller, G. H., Ahrens, M. J., & Winans, R. E. 2001, *OLEB*, 31, 15
 Bowden, S. A., Court, R. W., Milner, D., et al. 2008, *J. Anal. Appl. Pyrolysis*, 82, 312
 Bowden, S. A., Parnell, J., & Burchell, M. J. 2009, *IJAsB*, 8, 19
 Cable, M. L., Hörst, S. M., Hodyss, R., et al. 2012, *ChRv*, 112, 1882
 Cline, C. J., & Cintala, M. J. 2022, *M&PS*, 57, 1441

Gibbons, R. V., Morris, R. V., Horz, F., & Thompson, T. D. 1975, *LPSC*, 3, 3143
 Hashizume, H. 2015, *Life*, 5, 637
 Hashizume, H., van der Gaast, S., & Theng, B. K. G. 2010, *CIMin*, 45, 469
 He, C., Hörst, S. M., Lewis, N. K., et al. 2018a, *AJ*, 156, 38
 He, C., Hörst, S. M., Lewis, N. K., et al. 2018b, *ApJL*, 856, L3
 He, C., Hörst, S. M., Lewis, N. K., et al. 2019, *ESC*, 3, 39
 He, C., Hörst, S. M., Lewis, N. K., et al. 2020a, *PSJ*, 1, 51
 He, C., Hörst, S. M., Lewis, N. K., et al. 2020b, *NatAs*, 4, 986
 He, C., Hörst, S. M., Riemer, S., et al. 2017, *ApJL*, 841, L31
 Hedgepeth, J. E., Neish, C. D., Turtle, E. P., et al. 2020, *Icar*, 344, 113664
 Hörst, S. M. 2017, *JGRE*, 122, 432
 Hörst, S. M., He, C., Lewis, N. K., et al. 2018, *NatAs*, 2, 303
 Hörz, F. 1970, A Small Ballistic Range for Impact Metamorphism Studies TN D-5787/A-3181, NASA Ames Research Center <https://ntrs.nasa.gov/api/citations/19700017257/downloads/19700017257.pdf>
 Kraus, R. G., Senft, L. E., & Stewart, S. T. 2011, *Icar*, 214, 724
 Martins, Z., Price, M. C., Goldman, N., Sephton, M. A., & Burchell, M. J. 2013, *NatGe*, 6, 1045
 Moran, S. E., Hörst, S. M., Vuitton, V., et al. 2020, *PSJ*, 1, 17
 Neish, C. D., Lorenz, R. D., Turtle, E. P., et al. 2018, *AsBio*, 18, 571
 Pearce, B. K. D. 2023, Chromatogram Peak Integrator, v1.0, Zenodo, doi:10.5281/zenodo.10210586
 Pearce, B. K. D., He, C., & Hörst, S. M. 2022, *ESC*, 6, 2385
 Pearce, B. K. D., Hörst, S. M., Sebree, J. A., & He, C. 2024, *PSJ*, 5, 23

Pearce, B. K. D., Molaverdikhani, K., Pudritz, R. E., Henning, T., & Hébrard, E. 2020, [ApJ](#), **901**, 110
Pierazzo, E., Vickery, A. M., & Melosh, H. J. 1997, [Icar](#), **127**, 408
Poggiali, G., Fornaro, T., Potenti, S., Corazzi, M. A., & Brucato, J. R. 2020, [FrASS](#), **7**, 18

Sebree, J. A., Roach, M. C., Shipley, E. R., He, C., & Hörst, S. M. 2018, [ApJ](#), **865**, 133
Singh, S. V., Vishakantaiah, J., Meka, J. K., et al. 2020, [Molecules](#), **25**, 5634
Trainer, M. G., Pavlov, A. A., DeWitt, H. L., et al. 2006, [PNAS](#), **103**, 18035
Zahnle, K., Schenk, P., Levison, H., & Dones, L. 2003, [Icar](#), **163**, 263